Local structure of hole-doped manganites: influence of temperature and applied magnetic field

2002 J. Phys.: Condens. Matter 14 1967

(http://iopscience.iop.org/0953-8984/14/8/324)

INSTITUTE OF PHYSICS PUBLISHING JOURNAL OF PHYSICS: CONDENSED MATTER

J. Phys.: Condens. Matter **14** (2002) 1967–1974 PII: S0953-8984(02)30231-5

Local structure of hole-doped manganites: influence of temperature and applied magnetic field

Carlo Meneghini[1,2,7], **C Castellano**[3], **S Mobilio**[2,4], **Ashwani Kumar**[5], **S Ray**[5] **and D D Sarma**[5,6]

[1] INFM-GILDA c\o ESRF, Grenoble, France
[2] Dip. di Fisica 'E Amaldi', Universitá di Roma Tre, Via della Vasca Navale 84, I-00146 Roma, Italy
[3] Dip. di Fisica Universitá di Roma 'La Sapienza', P.le Aldo Moro 1, I-00100 Roma, Italy
[4] Laboratori Nazionali di Frascati, INFN, PO Box 13, I-00044 Frascati, Italy
[5] Solid State and Structural Chemistry Unit, Indian Institute of Science, Bangalore 560012, India
[6] Jawaharlal Nehru Centre for Advanced Scientific Research, Bangalore 560 064, India

E-mail: meneghini@fis.uniroma3.it

Received 31 October 2001
Published 15 February 2002
Online at stacks.iop.org/JPhysCM/14/1967

Abstract

We report an extended x-ray absorption fine-structure investigation on the Mn K absorption edge in $La_{1-x}Ca_xMnO_3$ as a function of temperature and magnetic field. The results provide microscopic evidence that the modifications in the local structure around Mn atomic sites, as a function of temperature and applied magnetic field, are directly related to the magneto-transport properties of these materials.

1. Introduction

In recent times hole-doped manganese oxide perovskites with basic formula $A_{1-x}B_xMnO_3$ (where A is a lanthanide and B is a divalent metal) have attracted unprecedented attention owing to their very peculiar magneto-transport property, the so-called colossal magnetoresistance (CMR) [1]. It is believed that in these systems the CMR is due to an interplay between structural, magnetic and transport properties. Extensive experimental and theoretical efforts have been made in order to obtain a detailed understanding of this interplay. In particular, $La_{1-x}Ca_xMnO_3$ in the doping range $0.2 < x < 0.5$ is insulating in the high-temperature paramagnetic state, but becomes metallic in the low-temperature ferromagnetic state. The close interconnection between magnetism and metallic state for $T < T_c$ is well documented in terms of the double-exchange mechanism [2–4]. However, it is now generally accepted that the double-exchange mechanism alone is not sufficient to quantitatively explain the unusual magneto-transport properties and that the coupling between charge and lattice degrees of freedom [5–7] plays a

[7] Author to whom any correspondence should be addressed.

key role in producing both the insulating behaviour at $T > T_c$ and the CMR effect around the metal–insulator (MI) transition temperature, T_{MI}. The undoped compound $LaMnO_3$ exhibits a Jahn–Teller (JT) distortion around the Mn^{3+} ion. Such a JT distortion is absent from the other extreme compound $CaMnO_3$, where only Mn^{4+} ions are present. For the hole-doped system where both Mn^{3+} and Mn^{4+} sites are present, local JT polaronic distortions localize the charge carriers in the high-temperature insulating phase. The size and strength of such polaronic distortion are key points in such discussions; in the limit of strong coupling, often associated in the literature with the formation of small polarons, the charge carriers are trapped on the locally distorted sites and thus the conductivity is given by thermally activated hopping or tunnelling between such distorted sites. The other limit of weak coupling is associated with the formation of large polarons extending over a wide spatial range and having an itinerant character. In doped perovskites different experimental techniques [8–20] have provided evidence for the evolution from a strong-coupling insulating phase ($T > T_{MI}$) to a metallic phase ($T < T_{MI}$) in which structural distortions are progressively reduced.

In this scenario the mechanism through which an applied magnetic field (H) promotes the conductivity seems limited to the spin–charge coupling; it favours the charge hopping by enhancing the ferromagnetic order as described in the double-exchange theory. Even though spin–charge and charge–lattice coupling have been widely documented in the literature, only a few works have attempted to reveal a direct spin–lattice coupling [12, 20–23] in order to determine whether and how the sample magnetization affects the structural distortions directly, thereby influencing charge transport and contributing to the CMR effect.

The aim of the present work is to determine quantitatively the evolution of the Mn local environment across the MI transition in the absence and presence of an applied magnetic field, in order to relate directly the microstructural changes to the evolution of CMR effect. For this purpose, we have carried out detailed extended x-ray absorption fine-structure (EXAFS) investigations at the Mn K edge in $La_{1-x}Ca_xMnO_3$ compounds, as a function of temperature, doping and magnetic field. Our results, in agreement with previous EXAFS experiments [11, 15–19], confirm the peculiar temperature dependence of the Mn–O Debye–Waller (DW) factor across the T_{MI}, unambiguously indicating an increase in the electron–phonon interaction in the insulating phase. In addition, they definitively assess the percolative nature of the insulator to metal transition and quantify the residual distortions in the low-temperature FM phase. These results, in agreement with recent EXAFS data on similar compounds [23], reveal that the application of a magnetic field modifies the evolution of JT distortions across the T_{MI} and that these changes are directly related to the magnetoresistance effect.

2. Experimental method and data analysis

Two samples of $La_{1-x}Ca_xMnO_3$, $x = 0.25$ and 0.33, were prepared by the conventional solid-state method using La_2O_3, $CaCO_3$ and Mn_3O_4. Samples were characterized by x-ray diffraction, resistivity, ac susceptibility and magneto-resistance measurements (figures 3(a) and (b)). Mn K-edge EXAFS data were recorded in transmission geometry at the CRG-GILDA beam line [24] at ESRF (Grenoble). Measurements were carried out between 77 and 360 K with a sampling step of 10 K in the neighbourhood of T_{MI}. For each sample two temperature runs were performed on cooling with $H = 0$ and 1.1 T, taking care to measure at the same temperature with and without the magnetic field. The EXAFS oscillations, $\chi(k)$ were extracted from XAS data (figure 1(a)) using a standard procedure [25, 26]. The k^2-weighted $\chi(k)$ data were Fourier transformed (FT) in the k range of 2.5–15 $Å^{-1}$ (figure 1(b)). The effect of decreasing the temperature is evident on both the EXAFS oscillations and FT by the increase in their amplitudes. While the first intense peak at about 1.5 Å in the FT corresponds to the

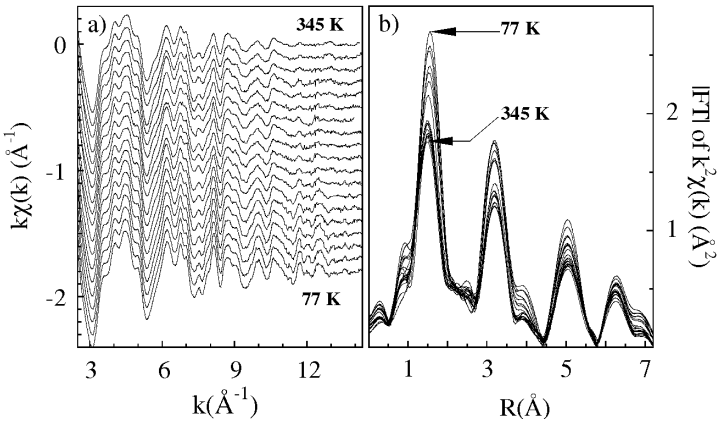

Figure 1. (*a*) k-weighted EXAFS data, $\chi(k)$, and (*b*) Fourier transforms of k^2-weighted $\chi(k)$ as a function of temperature for the $x = 0.25$ sample.

Mn–O bond lengths, the second one at about 3.2 Å has contributions not only from Mn–La/Ca and Mn–Mn (along the cube edge) pairs, but also includes multiple-scattering contributions from the almost collinear Mn–O–Mn triplets. We restrict our analysis to the Mn–O first shell by inverse Fourier transforming (Fourier filtering) the data in the range 0.5–2.6 Å. The filtered data were fitted using a standard single-scattering EXAFS formula [25] and theoretical amplitude and phase functions [27]. We find two Mn–O sub-shells are required to fit the data in the whole temperature range for both the samples (figure 2); one with about four oxygen neighbours at $R_a \simeq 1.93$ Å and the other with about two oxygen atoms at $R_b \simeq 2.05$ Å. In the final analysis the coordination numbers were fixed to $N^a_{\mathrm{MnO}} = 4$ and $N^b_{\mathrm{MnO}} = 2$ respectively, in agreement with a Q_3-type JT distortion of the MnO_6 octahedron. Fixing the coordination numbers reduces the uncertainty on the DW factors (σ^2), that were found to vary smoothly from about 1.7×10^{-3} Å^2 at LN temperature to about 2.5×10^{-3} Å^2 at RT, in agreement with other doped compounds [19] as well as pure $CaMnO_3$ [15], that is expected to be free from the Jahn–Teller distortion effect.

The possibility to distinguish a sub-shell structure in the first FT peak is relevant for the interpretation of the Mn EXAFS data in manganites and is a controversial issue in the literature [11, 15, 18, 19]. Such a possibility is related to the extension of the data in k-space, the windowing in the FT space, the number of independent fitting parameters [29] and the statistical noise in the experimental data. Figure 2(*a*) shows that the two-shell model improves the fit, reducing the residual by about a factor of three. However, the most suitable way to assess the accuracy and reliability of the best fit is a statistical analysis of the results, that is performing a χ^2- and an F-test on the results. Figure 2(*c*) shows the iso-χ^2 curves in the space of R_a and R_b parameters calculated using the CONTOUR option in the MINUIT package [28], for the $x = 0.25$ sample measured at LN temperature. Starting from a minimum ($\times$), each curve depicts a 5% increase in the best-fit reduced χ^2 [29]. Two local minima are evident in the figure: one, with $R_a \approx R_b \approx 1.965$ Å and a larger DW factor ($\sigma^2 = 2.6 \times 10^{-3}$ Å^2), means a single-shell MnO distribution; the other, with $R_a \approx 1.925$ Å, $R_b \approx 2.04$ Å and $\sigma^2 = 1.7 \times 10^{-3}$ Å^2, improves the reduced χ^2 by about 10%, so demonstrating that a bimodal distribution improves the fitting. An F-test ensures that this improvement is statistically significant.

The possibility that such a bimodal distribution shares a more complex sub-shell structure cannot be excluded. However an F-test, according to [29], shows that, in our data, adding a third shell in the fitting is not statistically significant. Nevertheless, the longer Mn–O distance,

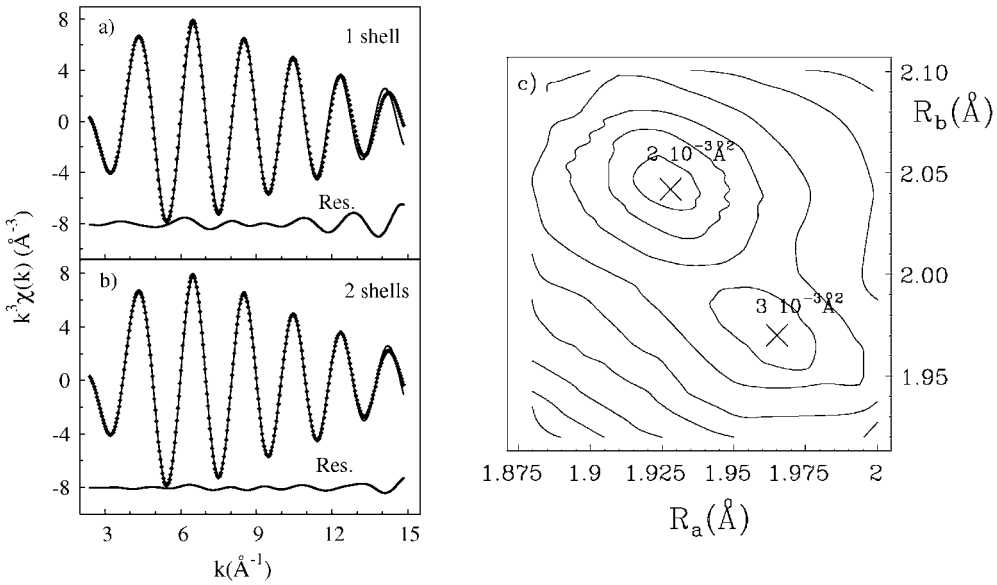

Figure 2. Example of fitting k^3-weighted filtered EXAFS data ($T = 77$ K) with one (*a*) or two (*b*) shells. Experimental (· · · · · ·) data and theoretical (——) curves are shown. The residuals (Res. $= k^3(\chi_{exp} - \chi_{th})$) are shown, shifted for clarity. Panel (*c*) reports the iso-χ^2 curves for the fit as a function of R_a and R_b parameters (see the text). The values of the DW factors in the two minima (×) are reported.

$R_b = 2.08$ Å, that we find for $x = 0.25$ in the insulating phase coincides with the value obtained by averaging the two long Mn–O bond distances (2.01 and 2.13 Å) as reported in [19]. Moreover, the $\sigma^2 \sim 2.5 \times 10^{-2}$ Å^2 found in the single-shell local minimum is in agreement with the value reported in [15], which points to the consistency of our results with previous ones.

The panels in figures 3(*c*), (*d*) report the two Mn–O coordination distances, R_a and R_b as a function of temperature obtained with $H = 0$ (open symbols) and $H = 1.1$ T (filled symbols).

3. Results and discussion

The changes in the $R_i(T)$ as a function of temperature (figures 3(*c*) and (*d*)) describe the structural evolution across the insulator–metal as well as paramagnetic–ferromagnetic transitions. The average Mn–O bond length, $\overline{R} = (4R_a + 2R_b)/6$, is about 1.97 and 1.96 Å, respectively, for $x = 0.25$ and 0.33 samples. In contrast, for both the samples, R_b decreases and R_a weakly increases on lowering T through T_{MI}, so the amplitude of the distortion, $\Delta R = R_b - R_a$, decreases from 0.16 (0.15) to 0.11 (0.10) Å in the $x = 0.25$ (0.33) sample. This, in agreement with experimental [19] and theoretical [30] findings, points out the transition from a stronger-coupling regime, characterized by larger distortions of the MnO_6 octahedron, to a weaker- (intermediate-) coupling regime, having smaller MnO_6 octahedron distortions. The quantity $\delta_{JT} = \sqrt{\frac{1}{6}\sum_{i=1}^{N}(R_{\mathrm{MnO}_i} - \overline{R}_{\mathrm{MnO}})^2}$ (where $N = 6$), reported in figures 3(*e*) and (*f*), quantifies the *local* JT distortion of the MnO_6 octahedron as a function of temperature and applied magnetic field, across the MI transition. These values are somewhat larger than the long-range coherent JT distortions obtained by diffraction techniques [9, 10]. In the paramagnetic regime the amplitude of the JT effect observed in our data is reduced with

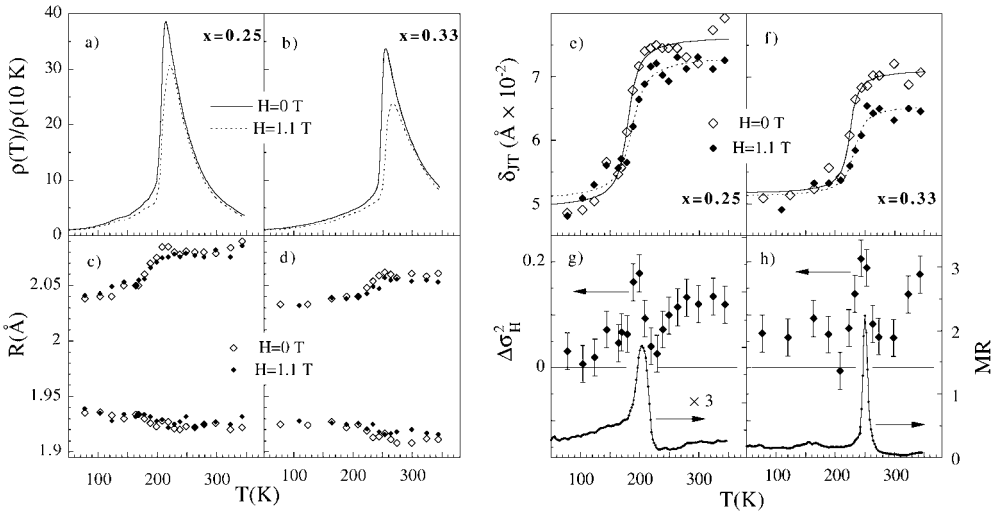

Figure 3. (*a*), (*b*) Resistivity, (*c*), (*d*) bimodal distribution of Mn–O bond lengths and (*e*), (*f*) local Jahn–Teller distortions of the MnO_6 octahedron in the absence ($H = 0$ T) and presence ($H = 1.1$ T) of magnetic field as a function of temperature. In panels (*g*) and (*h*), the relative variations in the DW factors ($\Delta\sigma_H^2 = (\sigma_H^2 - \sigma_0^2)/\sigma_H^2$) and magnetoresistance ($MR = (R_H - R_0)/R_H$) as a function of temperature are shown. Panels (*a*), (*c*), (*e*) and (*g*) ((*b*), (*d*), (*f*) and (*h*)) refer to the $x = 0.25$ (0.33) sample.

respect to that measured in fully distorted $LaMnO_3$ (in which $\delta_{JT} \approx 0.1$ Å) by a factor roughly equal to the chemical concentration of Ca, in agreement with the hypothesis of large distortions localized on each Mn^{3+} site (small polaron). This average distortion is relatively insensitive to T away from T_{MI}, with a considerably larger magnitude in the high-temperature phase, clearly pointing out the presence of larger lattice distortions in the insulating state as expected for a stronger-coupling regime. $\delta_{JT}(T)$ decreases rapidly only in the vicinity of T_{MI}, closely following the rapid decrease of resistivity with temperature. This effect signals the progressive reduction of charge–lattice coupling through the transition.

The amplitude of the JT distortion and its evolution through the transition represents an important parameter in the physics of CMR compounds. These results definitively prove that relatively large distortions remain in the FM–metallic phase, reaching about 50% of that found in fully JT-distorted $LaMnO_3$ compounds. The reductions of δ_{JT} and ΔR across the transition definitively confirm the transition from a single-site strong-coupling regime (small polarons) to an intermediate-coupling regime in which weaker distortions of MnO_6 octahedra are spread over a few (two to four) neighbour sites (large polarons) [7, 13, 14, 19, 30]. It is evident that present experimental results are clearly in contrast to the models envisaging complete removal of the distortions and full delocalization of charges and a complete vanishing of JT distortions.

Another important conclusion drawn from the data reported in figures 3(*a*)–(*f*) is that most of the structural changes occur mainly within the metallic region, starting from T_{MI}. It is also clear from these figures that the lattice distortions are consistently suppressed, though only weakly, on application of magnetic field of just 1.1 T. To quantify the structural effects induced by T and H, we characterized the transition from strong- to weak-coupling regimes in terms of some empirical parameters using the phenomenological relation

$$\delta_{JT}(T) = \frac{A}{\pi}\mathrm{arctg}\left(\frac{T - T_o}{\Delta T}\right) + \overline{\delta}_{JT} \tag{1}$$

Table 1. Empirical parameters characterizing the evolution of $\delta_{JT}(T)$ across the MI transition.

x	H (T)	A (Å)	T_o (K)	ΔT (K)	$\overline{\delta}_{JT}$ (Å)
0.25	0	0.027(2)	179(2)	13(3)	0.063(2)
	1.1	0.023(2)	187(3)	17(2)	0.062(2)
0.33	0	0.020(1)	224(2)	10(3)	0.061(2)
	1.1	0.015(2)	232(3)	14(3)	0.058(1)

to fit the $\delta_{JT}(T)$ data. Here A represents the variation of the amplitude of the JT distortion across the transition, T_o is the mean temperature which characterizes the cross-over temperature for the coupling strength and ΔT gives an estimate of the transition sharpness. The best-fit results so obtained are reported in table 1. Assuming that larger distortions indicate a larger number of strongly coupled sites and/or trapped carriers, $\delta_{JT}(T)$ describes how the average electron–phonon strength evolves as a function of temperature. With such an assumption, the quantity $P(T) = 0.5 + \frac{1}{\pi}\arctan\left(\frac{T-T_o}{\Delta T}\right)$ can be interpreted as the probability of having strongly coupled, heavily distorted Mn sites, where $P(T \gg T_o) \sim 1$ and $P(T \ll T_o) \sim 0$ would indicate the maximum and minimum numbers of distorted sites, respectively. Within this model the quantity $P(T_{MI})$, indicating the fraction of heavily distorted sites (thus of trapped carriers) at T_{MI}, is higher than 85–90% in both the samples. This demonstrates that a relatively small fraction of free charge carriers, proportional to the undistorted sites, produces the turn-over in resistivity giving rise to the MI transition. This result strongly supports that the sharp drop in resistivity derives from a percolative effect through domains of weakly distorted sites (weakly coupled itinerant charge carriers) microscopically dispersed into the heavily coupled insulating phase in agreement with the phase separation model in the neighbourhood of T_{MI} recently emphasized by several authors (see [31, 32] and references therein).

From the parameters given in the table 1, it is clear that the effect of the applied magnetic field on $\delta_{JT}(T)$ is similar for both the samples. The applied magnetic field shifts T_o towards higher temperatures by about 10 K, in agreement with [23]. Moreover, it increases ΔT, making the structural transition broader, and also reduces the overall distortion amplitude. These results, when compared with the resistivity in both the absence and presence of magnetic field (see figures 3(*a*), (*b*)), indicate that the effects produced by the applied magnetic field on the magneto-transport properties also have a counterpart in the local structure around Mn ions: that the drop in JT distortions as a function of temperature and magnetic field closely follows the onset of FM–metallic state with and without magnetic field.

Most convincing evidence of structural effects of H and its relation to magneto-transport properties is reported in figures 3(*g*) and (*h*), where the relative variation of the DW factors, $\Delta\sigma_H^2 = (\sigma_{H=0}^2 - \sigma_{H=1.1}^2)/\sigma_{H=1.1}^2$, is plotted. To obtain $\Delta\sigma_H^2$, we used the data collected with $H = 1.1$ T as a model to extract experimental amplitude and phase functions, which were used to fit EXAFS data collected in the absence of magnetic field, at each temperature. The analysis of EXAFS data of a sample using experimental backscattering amplitude and phase functions, extracted from EXAFS data collected on a *model* sample, is largely agreed as the most sensitive and accurate method to quantify weak differences between chemically similar samples. Further, as the two data sets ($H = 0$ and 1.1 T) were collected in the same experimental conditions and treated using the same procedure, we expect that systematic errors from measurements and/or data treatment are temperature independent, thus they may affect the absolute values of $\Delta\sigma_H^2$ but not its overall behaviour. The quantity $\Delta\sigma_H^2$ reported in figures 3(*g*) and (*h*) should be considered as the microscopic structural counterpart of the magnetoresistance effect MR $= (R_0 - R_H)/R_H$, reported in the same panels for the sake

of comparison. It is clear that the peak in $\Delta\sigma_H^2$ follows the peak in MR as a function of temperature, as is evident from the correlated shifts of $\Delta\sigma_H^2$ and MR between the two samples by nearly 40 K.

These results, in agreement with the recent results [23], definitively establish the strict relation between local distortions around Mn and evolution of magneto-transport properties: reduced resistivity, shift of the Curie temperature and evolution of the structural distortions upon the application of a magnetic field are intimately related effects. Structural modifications induced by magnetic field have also been pointed out in magnetostriction measurements [21, 22]. However, EXAFS results focus on the *local* distortions around Mn, which are incoherent, while magnetostriction, in contrast, is a coherent volume effect. The amplitude of the magnetostriction effect, $\Delta V/V \approx 10^{-4}$ [21, 22], is several orders of magnitude smaller than the local effect observed in our EXAFS data, which is $\approx 10^{-1}$. This finding definitively demonstrates that the distortions of the Mn local environment play a dominant role in determining the magneto-transport properties of hole-doped perovskites.

The $\Delta\sigma_H^2$ values at high temperatures do not decay to zero, but instead increase to quite large values 50–60 K above the first maximum discussed above. This effect has been consistently observed in all the samples investigated by us and also in an independent experiment [20]. The growth of $\Delta\sigma_H^2$ in the PM phase suggests that the structural effect of an external magnetic field cannot be simply explained with a rigid shift of the structural transition [23], but it involves more interesting microscopic changes. We suggest interpreting such an effect with the enhancement of the Debye temperature under applied magnetic field in the PM–insulating phase. A possible path for this could be weakening of charge–lattice coupling through the softening of spin polarons. This hypothesis could be confirmed by monitoring the shift of vibrational frequencies under applied magnetic field by Raman and/or IR spectroscopies. In this regard, it is worthwhile to note that pressure-induced hardening of vibrational frequencies has been recently reported [33] as a consequence of the pressure-induced reduction of charge–lattice coupling, and it is well known that applied pressure and magnetic field have a similar effect, at least in the low-/intermediate-pressure and field regions [34].

4. Conclusions

Our results describe and quantify the evolution of Mn *local* distortions through the MI transition and the microstructural effects induced by an applied magnetic field, definitively showing that the modifications of the local structure are intimately related to the evolution of magneto-transport properties and in particular to the MR effect. Furthermore the observed effects cannot be explained assuming that the applied magnetic field only enhances the charge hopping through the double-exchange mechanism, without the participation of the lattice; they imply that H also reduces the structural distortions through a softening of the electron–lattice coupling.

Acknowledgments

We thank Professor M L Fernandez-Gubieda of the Departemmento de Electricidad y Electrónica, Universidad del País Vasco, Bilbao, Spain, for susceptibility and magnetoresistance measurements. We acknowledge the technical support provided by F Campolungo, V Sciarra and V Tullio of the Laboratori Nazionali di Frascati dell'INFN. The GILDA project is financed by the Italian institutes CNR, INFM and INFN.

References

[1] Helmholt v R, Wecker J, Holzapfel B, Schultz L and Somwer K 1993 *Phys. Rev. Lett.* **71** 2331
[2] Zener C 1951 *Phys. Rev.* **82** 403
[3] Anderson P W and Hasegawa H 1955 *Phys. Rev.* **100** 675
[4] de Gennes P G 1960 *Phys. Rev.* **118** 141
[5] Millis A J, Littlewood P B and Shraiman B I 1995 *Phys. Rev. Lett.* **74** 5144
[6] Millis A J, Shraiman B I and Mueller R 1996 *Phys. Rev. Lett.* **77** 175
[7] Roder H, Zhang J and Bishop A 1996 *Phys. Rev. Lett.* **76** 1356
[8] Billinge S J L, Di Francesco R G, Kwei G H, Neumeier J J and Thompson J D 1996 *Phys. Rev. Lett.* **77** 715
[9] Radaelli P G, Cox D E, Marezio M, Cheong S-W, Schiffer P E and Ramirez A P 1996 *Phys. Rev. Lett.* **75** 4488
[10] Radaelli P G, Iannone G, Marezio M, Hwang H Y, Cheong S-W, Jorgensen J D and Argyriou D N 1997 *Phys. Rev.* B **56** 8265
[11] Tyson T A, de Leon J M, Conradson S D, Bishop A R, Neumeier J J, Röder H and Zang J 1996 *Phys. Rev.* B **53** 13 985
[12] De Teresa J M *et al* 1997 *Nature* **386** 256
[13] Louca D, Egami T, Brosha E L, Röder H and Bishop A R 1997 *Phys. Rev.* B **56** R8475
[14] Louca D and Egami T 1999 *Phys. Rev.* B **59** 6193
[15] Booth C H, Bridges F, Kwei G H, Lawrence J M, Cornelius A L and Neumeier J J 1998 *Phys. Rev.* B **57** 10 440
[16] Meneghini C, Cimino R, Pascarelli S, Mobilio S, Raghu C and Sarma D D 1997 *Phys. Rev.* B **56** 3520
[17] Yoon S, Liu H L, Schollerer G, Cooper S L, Han P D, Payne D A, Cheong S-W and Fisk Z 1998 *Phys. Rev.* B **58** 2795
[18] Subias G, Garcá J, Blasco J and Proietti M G 1998 *Phys. Rev.* B **57** 748
[19] Lanzara A, Saini N L, Brunelli M, Natali F, Bianconi A, Radaelli P G and Cheong S-W 1998 *Phys. Rev. Lett.* **81** 878
[20] Meneghini C, Castellano C, Mobilio S, Kumar A, Ray S and Sarma D D 1999 *Phys. Status Solidi* **215** 647
[21] Ibarra M R, Algarabel P A, Marquina C, Blasco J and García J 1995 *Phys. Rev. Lett.* **75** 3541
[22] De Teresa J M, Ibarra M R, Blasco J, García J, Marquina C, Algarabel P A, Arnold Z, Kamenev K, Ritter C and von Helmolt R 1996 *Phys. Rev.* B **54** 1187
[23] Cao D, bridges F, Booth C H and Neumeier J J 2000 *Phys. Rev.* B **62** 8954
[24] Pascarelli S, Boscherini F, D'Acapito F, Hrdy J, Meneghini C and Mobilio S 1996 *J. Synchrotron. Radiat.* **3** 147
[25] Lee P A, Citrin P H, Eisenberger P and Kinkaid B M 1981 *Rev. Mod. Phys.* **53** 769
[26] Lengeler B and Eisenberger P 1980 *Phys. Rev.* B **21** 4507
[27] McKale A G 1988 *J. Am. Chem. Soc.* **110** 3763
[28] James F 1994 *MINUIT: Function Minimization and Error Analysis. Reference Manual* version 94.1, Program Library D506, CERN
[29] Lytle F W, Sayers D E and Stern E A 1989 *Physica* B **158** 701
[30] Cataudella V, De Filippis G and Iadonisi G 2001 *Phys. Rev.* B **63** 052406
[31] Jaime M, Lin P, Chun S H, Salamon M B, Dorsey P and Rubinstein M 1999 *Phys. Rev.* B **60** 1028
[32] Moro A, Yunoki S and Dagotto E 1999 *Science* **283** 2034
[33] Congeduti A, Postorino P, Caramagno E, Nardone M, Kumar A and Sarma D D 2001 *Phys. Rev. Lett.* **86** 1251
[34] Morimoto Y, Asamitsu A and Tokura Y 1995 *Phys. Rev.* B **51** 16 491